Electron-Interaction Effects on the Soft X-Ray Emission Spectrum of Metals. I. Formalism and First-Order Theory*†

PIERRE LONGE‡
Institut de Physique, Université de Liège, Sart Tilman, Belgium
AND
ARNOLD J. GLICK§
Service de Physique Théorique, Centre d'Etudes Nucléaires de Saclay, BP no. 2-91, Gif-sur-Yvette, France, and Faculté des Sciences, Université de Paris, Orsay, France

(Received 8 May 1968)

The soft x-ray emission spectrum of metals is studied using a diagrammatic many-body perturbation theory to account for the interactions between electrons. On the basis of a one-electron model, the emission spectrum gives a direct measure of the Fermi energy and is simply related to the conduction-electron density of states. In actual metals, however, the spectra are strongly modified by electron interactions, and these relations are no longer valid. A low-energy tail is introduced in place of a sharp emission threshold, and a satellite band appears which is associated with plasmon excitation in the metal. The first-order theory described here shows that certain interference terms play an important role in determining the emission intensity. For sodium, a satellite band is obtained with maximum intensity between 1% and 2% of the parent band, in agreement with observations by Rooke. The low-energy tail has a similar strength in the region of the satellite. The first-order theory, however, breaks down in the region of the parent band spectrum.

I. INTRODUCTION

SOFT x-ray spectroscopy is a useful tool for obtaining information about the conduction electrons in metals.[1–5] This information has usually been interpreted in terms of a one-electron model, though it is recognized that significant corrections must be made for many-electron effects. This paper is the first of several in which we employ many-body theory to study systematically the new features which electron interactions introduce into the emission spectrum of a metal for which the free-electron approximation is valid, such as for the alkali metals. In particular, the present article contains a description of the formalism to be employed and a calculation of the $L_{2,3}$ emission spectrum of sodium to first order in the effective interaction. As will be seen below, the first-order theory encounters certain divergence difficulties when applied to the "main" or "parent band" portion of the spectrum, and the second article of this series[6] will describe a renormalized theory from which the divergences are eliminated. However, the first-order theory is useful for gaining insight into the structure of the theory and the physical processes which contribute to the emission. It will be seen that several early treatments[7–9] of many-body effects in emission were incomplete and neglected important interference terms. When these terms are included, one obtains an emission spectrum for the low-energy tail of the main band and for the "plasmon satellite" band which are in good accord with experiment.

Soft x-ray emission occurs after a localized electron is somehow removed from an energy level below the conduction band of the metal, (say by x-ray or fast-electron bombardment). An electron in the conduction band can then drop into the localized hole state, giving up its energy as x radiation. The elementary theory of this process,[1,2,10] which is based on a one-electron Bloch model, is illustrated in Fig. 1. The radiation intensity depends on the rate of electron transitions induced by the electromagnetic field. If the field is treated semiclassically, it couples to the electron through the momentum operator $\mathbf{n}\cdot\mathbf{p}$, where $\mathbf{n}$ is a unit polarization vector in the direction of the vector potential. Then (with $\hbar=1$) the emission intensity is proportional to

$$I_0(\omega)=(\omega/l)\sum_{i,f}\delta(\omega+\epsilon_f-\epsilon_i)\,|\,\langle\varphi_f\,|\,\mathbf{n}\cdot\mathbf{p}\,|\,\varphi_i\rangle\,|^2, \quad (1)$$

where one sums over all possible final states and averages over initial states, l being the number of initial states. The initial state is a hole in a localized bound level about one ion in the metal. If there are several levels close together in energy, then an average is necessary (as for $L_{2,3}$ emission). In this model, the final state is a hole in

* A brief preliminary report of this work appeared in Phys. Rev. Letters **15**, 589 (1965).

† Supported in part by U.S. Air Force Office of Scientific Research under Grant No. AF-AFOSR-735-65 to the University of Maryland.

‡ Chercheur I.I.S.N., Belgium.

§ Permanent address: University of Maryland, College Park, Md.; National Science Foundation Postdoctoral Fellow 1967–68.

[1] H. W. B. Skinner, Phil. Trans. Roy. Soc. London **A239**, 95 (1940).

[2] D. H. Tomboulian, in *Handbuch der Physik*, edited by S. Flugge/Marburg (Springer-Verlag, Berlin, 1957), Vol. 30, pp. 246–304.

[3] Y. Cauchois, *Les Spectres de Rayons X et la Structure Électronique de la Matière* (Gautier-Villars, Paris, 1948).

[4] L. G. Parratt, Rev. Mod. Phys. **31**, 616 (1959).

[5] A. Appleton, Contemp. Phys. **6**, 50 (1964).

[6] S. M. Bose, A. J. Glick, and P. Longe, (to be published); see also S. M. Bose, Ph.D. thesis, University of Maryland, 1967 (unpublished); A. J. Glick, P. Longe, and S. M. Bose, in *Proceedings of the Conference on Soft X-Ray Spectroscopy and the Band Structure of Metals and Alloys, 1967* (Academic Press Inc., New York, to be published).

[7] P. T. Landsberg, Proc. Phys. Soc. (London) **A62**, 806 (1949).

[8] J. Pirenne and P. Longe, Physica **30**, 277 (1964).

[9] R. A. Ferrell, Rev. Mod. Phys. **28**, 308 (1956).

[10] F. Seitz, *The Modern Theory of Solids* (McGraw-Hill Book Co., New York, 1940), see pp. 350-352.

any one of the normally occupied conduction states in the Fermi sea. Since the δ function in Eq. (1) conserves energy, the sum over final states becomes proportional to the conduction electron density of states $N(E)$ times a sum over squared matrix elements $P(E)$ for final states with energy between E and $E+dE$. Here E is related to the x-ray frequency ω by $E=\hbar\omega+E_B$, where E_B is the discrete (negative) energy of the low-lying state measured from the bottom of the conduction band. For a metal with a spherical Fermi surface, $N(E)$ is proportional to $E^{1/2}$ from 0 to the Fermi energy E_F, and vanishes elsewhere. Symmetry considerations[11] indicate that for metals where the conduction electrons have mostly s-wave character near the ions, the leading term of $P(E)$ is proportional to E for transitions to an even-parity state (K-shell emission) and is constant for transitions to an odd state (L-shell emission). Thus the spectrum is expected to exhibit $E^{3/2}$ or $E^{1/2}$ behavior, respectively, with onset at $E=0$ and a rapid fall at $E=E_F$. Thus, according to the one-electron model, the spectrum gives a measure of the width of the conduction band. In addition, the energy dependence of the emission intensity gives information about the density of states of conduction electrons with the appropriate symmetry about the ions.

Experimental emission spectra[1,12–14] resemble the spectra of the one-electron model, but also exhibit qualitatively different features. We will not concern ourselves here with lattice effects which modify $N(E)P(E)$ but which can still be included within a one-electron description. These features even appear for metals such as the alkalis for which lattice effects on the conduction electrons are negligible. The L emission spectrum of sodium is shown in Fig. 2(a) (after Ref. 13). Note that there is a low-energy tail which obscures the $E=0$ onset. This tailing appears to be a common feature of all such spectra.[1] In addition there is a structure at the high-energy end of the spectrum, though this feature did not appear in the spectrum found for sodium by Cady and Tomboulian.[14] Rooke[15] has observed a weak satellite band shifted down in energy by about 5 eV from the band shown in Fig. 2(a). Rooke has not yet published his sodium result,

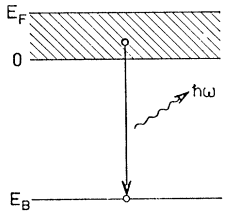

FIG. 1. One-electron model of the soft x-ray emission process.

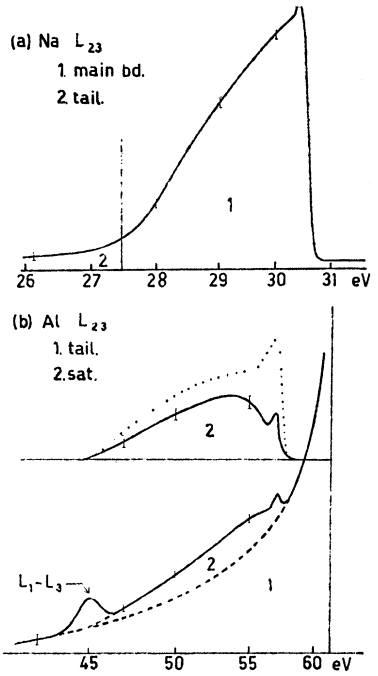

FIG. 2. Experimental soft x-ray emission spectra: (a) L emission spectrum of sodium after Ref. 13, showing the main or parent band and the low-energy tailing. (b) The tailing and plasmon satellite band in the spectrum of aluminum according to Rooke, Ref. 15.

but an analogous satellite for aluminum is pictured in Fig. 2(b) (after Ref. 15).

It is apparent from Fig. 1 that a purely one-electron description cannot explain any emission intensity for $E<0$. The tailing and the low-energy satellite must therefore be cooperative effects due to transitions in which some of the energy of the radiating electron is retained by the metal, and taken up by other conduction electrons. Two earlier treatments have shown how interactions can give rise to the tailing. Landsberg[7] noted that the initial electron hole in the bound state and the final hole in the conduction band are not really well-defined states. Because of electron-electron scatterings these states have a finite lifetime or width. Consequently, the δ functions in Eq. (1) should be replaced by suitable Lorentzian distributions which round the spectrum and supply a tail. It can be shown that the width of the bound state is not very significant in this case. Electromagnetic self-energy processes provide a bound-state width in sodium on the order of 10^{-6} eV, while even the more important Coulomb self-energy processes provide a width of only 10^{-3} eV. The width of a conduction band state, however, depends on its energy. At the Fermi energy it vanishes, but towards the bottom of the conduction band it grows to almost 1 eV. As a result there is a substantial tail introduced on the low-energy side of the spectrum, with little effect on the high-energy side, in qualitative agreement with experiment. A second mechanism which gives rise to a tailing was discussed by Pirenne and Longe.[8] It is based

[11] H. Jones, N. F. Mott, and H. W. B. Skinner, Phys. Rev. **45**, 379 (1934).
[12] *Landolt-Börnstein Tables* (Springer-Verlag, Berlin, 1955), sixth ed., Vol. 1, Part 4, pp. 769–867.
[13] R. S. Crisp and S. E. Williams, Phil. Mag. **6**, 365 (1961).
[14] W. M. Cady and D. H. Tomboulian, Phys. Rev. **59**, 381 (1941).
[15] G. A. Rooke, Phys. Letters **3**, 234 (1963).

on the observation that the initial state, with a hole in the ion core, appears to the conduction electrons as a localized charged impurity. After the transition the localized impurity disappears and the conduction band hole can move rapidly away through the crystal. Thus the fields seen by the electrons change suddenly and so do their wave functions. As a result Auger processes can occur during the emission of the x-ray, leaving additional holes in the conduction band and electrons in excited levels above the Fermi level. Since these electrons require energy to be excited, there is less energy left for the x-ray and a low-energy tail results. They find that this process is of the same order of magnitude as the Landsberg process. Both calculations are carried out using a static screened Coulomb force between electrons. When the screening length is taken as 0.68 Å, as suggested for sodium by the Thomas-Fermi model, they find good agreement with experiment. The strength of the tailing predicted by the combined Landsberg and Pirenne-Longe processes seems to be of the correct order of magnitude when compared with the experimental spectrum of Fig. 2. However, neither of these theories explains the presence of the low-energy satellite band observed by Rooke.[15]

The existence of such a satellite band was predicted by Ferrell[7] on the basis of Bohm-Pines theory. A more detailed application of Bohm-Pines theory was reported by Brouers,[16] and more recently Ferrell[17] used a semiclassical approach. The calculated strength of the satellite is found to be in good agreement with Rooke's observation, provided one accounts for a strong cancellation between a term in which the plasmon is coupled to the initial hole in the localized bound state and a term in which it is coupled to the final hole in the conduction band.[18,19] Thus, plasmon excitation can also be interpreted as a result of the sudden change in the charge distribution seen by the other electrons as the localized bound-state hole suddenly changes into a conduction band hole. Since plasmon excitation requires a certain minimum energy, the satellite emission band is shifted by a corresponding amount below the main emission band.

While the above calculations seem to contain the essential features needed for a qualitative description of observed L-shell emission spectra, it would be desirable to develop a much more unified and systematic treatment of the problem. Recently, some attempts along these lines have been reported.[18,20,21] Here we present the details of the method sketched in Ref. 18 along with corrected results. The calculations are based on Green's functions and many-body perturbation theory. The results obtained with these methods should also be of interest as a check on many-body theory as applied to real metals and to a case where not only electrons near the Fermi surface, but electrons throughout the whole conduction band, contribute.

In the next section, we present a general formulation of the problem from a many-particle point of view and in the third section details of the calculations are presented. The last section contains a summary of the results and a discussion of the difficulties which must still be resolved.

II. GENERAL FORMULATION

A. Emission Intensity

When the metal is considered as a many-body system, the emission intensity takes the form

$$I(\omega)=(\omega/l)\sum_{i,f}\delta(\omega+E_f-E_i)\mid\langle\Psi_f\mid\sum_{k=1}^{N}\mathbf{n}\cdot\mathbf{p}_k\mid\Psi_i\rangle\mid^2, \tag{2}$$

where the notation is similar to that of Eq. (1) except that the energies E_i and E_f and the corresponding states Ψ_i and Ψ_f are solutions of an N-particle Schrödinger equation, where the Hamiltonian H contains the interaction between electrons as well as with the nuclei. Since Ψ_i and Ψ_f are not ground states of the system, they have a finite lifetime to radiative decay. However, since the coupling to the radiation field is weak, we can treat it in linear approximation and obtain a transition rate of the type shown above in Eq. (2).

For later application, it is convenient to rewrite Eq. (2) using a representation of the δ function in terms of the real part of an integral over a parameter t

$$\delta(\omega+E_f-E_i)=(1/\pi)\ \mathrm{Re}\int_0^\infty dt\exp[-i(\omega+E_f-E_i)t].$$

With this expression, Eq. (2) becomes

$$I(\omega)=(\omega/\pi l)\ \mathrm{Re}F(\omega) \tag{3}$$

with

$$F(\omega)=\sum_{i,f}\int_0^\infty dt\,e^{-i\omega t}\langle\Psi_i\mid\theta^\dagger(t)\mid\Psi_f\rangle\langle\Psi_f\mid\theta(0)\mid\Psi_i\rangle, \tag{4}$$

where

$$\theta(t)=e^{iHt}\theta e^{-iHt}$$

and

$$\theta=\sum_{k=1}^{N}\mathbf{n}\cdot\mathbf{p}_k.$$

Applying closure to the sum over final states, we

[16] F. Brouers, Phys. Letters **11**, 297 (1964); Phys. Status Solidi **22**, 213 (1967).
[17] R. A. Ferrell, University of Maryland Technical Report No. 485, 1965 (unpublished).
[18] A. J. Glick and P. Longe, Phys. Rev. Letters **15**, 589 (1965).
[19] F. Brouers and P. Longe, Phys. Letters **26A**, 119 (1968).
[20] L. Hedin, Solid State Commun. **5**, 451 (1967); and in *Proceedings of the Conference on Soft X-Ray Spectroscopy and the Band Structure of Metals and Alloys, 1967* (Academic Press Inc., New York, to be published).
[21] R. G. Rystephanick and J. P. Carbotte, Phys. Rev. **166**, 607 (1968).

obtain

$$F(\omega)=\sum_i \int_0^\infty dt\, e^{-i\omega t}\langle \Psi_i \mid \theta^\dagger(t)\theta(0) \mid \Psi_i\rangle. \quad (5)$$

In this form there is no more reference to the final states which are implicitly contained in the l correlation functions

$$\langle \Psi_i \mid \theta^\dagger(t)\theta(0) \mid \Psi_i\rangle.$$

The function $F(\omega)$ will be calculated below with the aid of diagrammatic many-body perturbation theory.

B. Nonuniform System

These techniques must be applied to a nonuniform system. Translational invariance, which is usually invoked when studying a system of conduction electrons, cannot be assumed here because the initial state contains a localized excitation corresponding to the missing tightly bound core electron of the one-electron model. However, using the methods of Hubbard,[22] we will be led to a form of the theory which is formally the same as for the uniform system. We separate the Hamiltonian H into two parts

$$H_0=\sum_{k=1}^{N}[\mathbf{p}_k^2/2m+U(\mathbf{x}_k)+V_{\text{S.C.}}(\mathbf{x}_k)], \quad (6)$$

$$H'=\tfrac{1}{2}\sum_{k\neq k'}^{N} v(\mathbf{x}_k-\mathbf{x}_{k'})-\sum_{k=1}^{N} V_{\text{S.C.}}(\mathbf{x}_k), \quad (7)$$

where $U(\mathbf{x}_k)$ represents the Coulomb interaction between an electron and the N/Z nuclei, $v(\mathbf{x}_k-\mathbf{x}_{k'})$ is the Coulomb interaction between electrons, and $V_{\text{S.C.}}(\mathbf{x}_k)$ is the potential energy of a self-consistent field which must be determined. The Hamiltonian H_0 provides a set of one-electron states which satisfy the wave equation

$$[(\mathbf{p}^2/2m)+U(\mathbf{x})+V_{\text{S.C.}}(\mathbf{x})]u_i(\mathbf{x})=E_i u_i(\mathbf{x}). \quad (8)$$

Then H' can be taken as a perturbing Hamiltonian which gives rise to electron transitions which are represented in terms of Feynman-type graphs. As usual, one distinguishes between two types of lines in the diagrams—the directed line representing a particle in a state and the line of Coulomb interaction. These lines meet at vertices which consist of two particle lines, one coming in and the other leaving the vertex, and one interaction line which terminates at the vertex. In addition, to describe the second term of Eq. (7) one can introduce the "V points" at each of which an interaction line terminates. Using the convention with time flowing upwards, the instantaneous interaction lines will be horizontal and the particle lines are directed upward or downward depending, respectively, on whether they describe an electron in a state which is normally unoccupied in the N-particle ground state of H_0, or whether they describe an electron missing from a state which is normally occupied in the reference ground state. There also are passive particle lines whose end points are always associated with the same Coulomb interaction line and hence with the same instant of time.

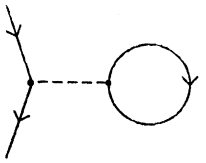

FIG. 3. Particle scattering by the simplest H part. The passive closed particle loop is equivalent to a symmetrized Hartree field.

Let us first consider the diagrams without any V points. These diagrams can contain what Hubbard[22] calls "H parts." These are parts of the graph which can be detached from the graph by cutting a single interaction line. A simple example of this type is the passive particle loop or bubble attached to a vertex by a Coulomb line as shown in Fig. 3. This term reduces to the symmetrized Hartree field. When the contribution of these graphs is calculated, one finds that the H parts enter as a factor of the form

$$\cdots\int d\mathbf{x}'v(\mathbf{x}-\mathbf{x}')H(\mathbf{x}'), \quad (9)$$

where $H(\mathbf{x}')$ represents the term resulting after the integration over any variables inside the H part of the graph. In the uniform-field case, with a uniformly smeared out positive charge background, one has

$$\int d\mathbf{x}'v(\mathbf{x}-\mathbf{x}')=0.$$

Since all points of space are equivalent, $H(\mathbf{x}')$ cannot depend on position and it must be constant. Thus all terms of the form (9) must vanish. In other words, the H parts are irrelevant to this case. For the nonuniform case it is useful to distinguish between the "improper H parts" which can be separated into another H part and a polarization part, and the "proper H parts" for which such a separation is impossible. Let us denote the contribution of such a proper H part by $H_{pr}(\mathbf{x})$. Hubbard showed that by setting $V_{\text{S.C.}}(\mathbf{x})$ equal to an integral of the type in Eq. (9), where $H(\mathbf{x})$ represents a sum of all the $H_{pr}(\mathbf{x})$, there are exact cancellations between the H part and the V-point contributions. Consequently, one can discard from the beginning all diagrams which contain any H parts or V points. One is thus led back to a formalism identical to that of the uniform case except that Eq. (8) is now used to define the one-electron states.

III. DETAILS OF THE CALCULATION

A. One-Electron Wave Functions

Thus $V_{\text{S.C.}}(\mathbf{x})$ as introduced by Hubbard appears as a generalized Hartree field. To a good approximation, however, it should be sufficient to keep only the simplest

[22] J. Hubbard, Proc. Roy. Soc. (London) **A244**, 199 (1958).

H part, which is the passive particle loop of Fig. 3. Then one has

$$V_{\text{S.C.}}(\mathbf{x}) = \int d\mathbf{x}\, v(\mathbf{x}-\mathbf{x}')\rho(x') \tag{10}$$

with

$$\rho(\mathbf{x}) = \sum_{i}^{\text{occ}} |u_i(\mathbf{x})|^2, \tag{11}$$

where the sum is only over the states occupied in the ground state of H_0. Then Eq. (8) becomes the usual Hartree equation where, however, the self-consistent potential is symmetized, and the same for all particles in the system.

For the core states, the solution of Eq. (8) is not difficult. Since we will be considering only the alkali metals, we can use the tight-binding approximation and also neglect the overlap of wave functions associated with different ions. Thus we will write the wave functions of level i for the ion situated at $\mathbf{l}$ as

$$u_{i\mathbf{l}}{}^B(\mathbf{x}) = u_i{}^B(\mathbf{x}-\mathbf{l}), \tag{12}$$

where the $u_i{}^B(\mathbf{x})$ are the simple atomic wave functions. These functions will be constructed using Slater's method[23] of shielding constants. The Schmidt orthogonalization procedure will be used to make them orthogonal as they should be because the Hartree field is symmetric. As we will see below, their energies do not enter the calculation explicitly. Even the energy separation E_B between the conduction band and the core level which is empty in the initial state always appears in the combination $\hbar\omega+E_B$ and hence only fixes a convenient origin for frequency.

At first sight, it would seem that it would be adequate to use plane waves for the conduction states. In fact, the conduction wave functions are practically plane in the region where the $u_{i\mathbf{l}}{}^B(\mathbf{x})$ are negligible, which for the alkali metals is a major part of the metallic volume Ω (more than 90% of the volume for sodium according to Wigner and Seitz[24]). However, x-ray emission is a process which occurs in the immediate neighborhood of an ion and, as has been shown by Jones, Mott, and Skinner,[11] even in the simple Bloch model the core part of conduction wave function plays an essential role. This core part arises as a consequence of the orthogonality of the wave function to the core states rather than as an effect of the ionic potential. In fact, if one considers the nonorthogonalized Slater wave function of the valence electron of an isolated alkali atom one finds that the inverse of the shielding constant is larger than the size of the Wigner-Seitz cell.[25] In the metal this function, therefore, becomes practically constant in each Wigner-Seitz cell. However, when the state is orthogonalized it regains its appropriate $3s$ character near the ion centers. It thus appears that the orthogonal plane wave (OPW) is particularly suitable for describing the conduction states. Thus we write

$$u_{\mathbf{k}}(\mathbf{x}) = (1/\sqrt{\Omega})e^{i\mathbf{k}\cdot\mathbf{x}} - \sum_{i}^{Z-1}\sum_{\mathbf{l}}^{N/Z} \bar{u}_{i\mathbf{l}}{}^B(\mathbf{k})\, u_{i\mathbf{l}}{}^B(\mathbf{x}), \tag{13}$$

where the sum is over all core states and the $u_{i\mathbf{l}}{}^B(\mathbf{k})$ are the Fourier transforms of $u_{i\mathbf{l}}{}^B(\mathbf{x})$ with the property

$$u_{i\mathbf{l}}{}^B(\mathbf{k}) = e^{-i\mathbf{k}\cdot\mathbf{l}} u_i{}^B(\mathbf{k}). \tag{14}$$

If the Fermi surface is far from the boundaries of the first Brillouin zone it is not necessary to superpose on Eq. (13) any other terms like $u_{\mathbf{k}+\mathbf{g}}(\mathbf{x})$, where $\mathbf{g}$ is a reciprocal lattice vector. The correction for the normalization of the wave function is also negligible since the core states of the alkali metals are so strongly bound. We have compared $u_{\mathbf{k}=0}(\mathbf{x})$ given by Eq. (13) for sodium with the same wave function calculated by the method of Wigner and Seitz[24] and the agreement is very good. Fixing the energy zero at the bottom of the conduction band, the energies of the conduction state $u(\mathbf{x})$ become simply $E_k = k^2/(2m)$. Note that the OPW functions of Eq. (13) are not orthogonalized among themselves as would be required by Eq. (8). However there is little error introduced by this approximation. Indeed the core and conduction wave functions appear in matrix elements of the type $\langle u_j \mid A \mid u_{j'}\rangle$. When the two wave functions in this matrix element refer to conduction states, one has an integral which extends over the entire volume Ω of the metal. In this case the domain of nonorthogonality, i.e., the volume occupied by the core wave functions is negligible in comparison with the entire volume of integration. Indeed, one can simplify still further and replace the OPW functions of the conduction states by plane waves [see below Eqs. (15a), (15a′)]. If, on the other hand, one of the two wave functions describes a core state, then the orthogonality is crucial, and the full OPW function must be used.

For completeness, the explicit expressions for the $u_i(\mathbf{x})$ for sodium are given in Appendix A.

B. Diagrammatic Expansion

The function $F(\omega)$ defined by (5) can be expanded in the usual way[26] in terms of the interaction between electrons. Each order of perturbation theory can then be represented by a set of Feynman-type graphs. For a system with Coulomb interactions, it is useful to rearrange the series in terms of $V(\mathbf{k},\omega)$, the effective interaction between electrons. $V(\mathbf{k},\omega)$ contains the modification of the interaction due to polarization or dynamic screening by other electrons in the metal.

In this paper, we will limit ourselves to diagrams of

[23] J. C. Slater, Phys. Rev. **36**, 57 (1930).

[24] E. Wigner and F. Seitz, Phys. Rev. **43**, 804 (1933); **46**, 509 (1934).

[25] E.g., for atomic solium, the Slater shielding length for the $3s$ valence electron is 1.36 a.u. and the radius of the Wigner-Seitz cell of metallic sodium is 1.12 a.u.

[26] See, e.g., J. Hubbard, Proc. Roy. Soc. (London) **A240**, 539 (1957) or A. J. Glick, in *Lectures on the Many Body Problem*, edited by E. Caianiello (Academic Press Inc., New York, 1962).

order 0 and 1 in the effective interaction. The rules for calculating the contribution associated with each diagram are similar to those in Ref. 26; except for obvious modifications connected with the presence of core states. For convenience we will enumerate the rules in Appendix B.

The general diagram to be determined is shown in Fig. 4. In this figure and the ones which follow, the double line (always pointed downward) represents the missing electron, or hole, in any one of the core states. For present purposes, however, we need not consider all of the core states. Recall that we will be considering a particular emission band, the $L_{2,3}$ band of sodium. This band is associated with the excitation of an electron from the highest core level below the conduction band, i.e., the $2p$ level. Lower-lying states contribute to emission bands at higher energies, but the tails of these spectra will be negligible for the frequency range of present interest. In addition, the interaction between conduction electrons and the deep lying states should be a very weak effect, so that it should be possible to neglect all the core states except the three nearly degenerate $2p$ states. Thus from here on the double line and $u_i^B(\mathbf{x})$ will refer only to the three wave functions (A1c), where $i=1, 2, 3$ indicates the three spacial directions.

Also present in the diagrams are single directed lines. These lines always refer to a state in the conduction band. To represent a state which can be either a core level or in the conduction band, we use a single line accompanied by a dashed line as in Fig. 4. The two wavy lines, one entering and one leaving each term in Fig. 4, represent the interactions with the radiation field which occur at times 0 and t, with the convention that time increases upward. The line of bubbles represents the effective interaction between electrons.

The black box with the two wavy lines on the left side of Fig. 4 represents the operator $\theta^\dagger(t)\theta(0)$. Its mean value is calculated for a state containing one core vacancy which is represented by the double lines which enter and leave the box. The right side of Fig. 4 shows all of the graphs which contribute through order 0 and 1 in the effective potential.

The essential difference between the usual diagrammatic rules and those for the present problem are associated with the presence of the bound states and the consequent loss of momentum conservation at the

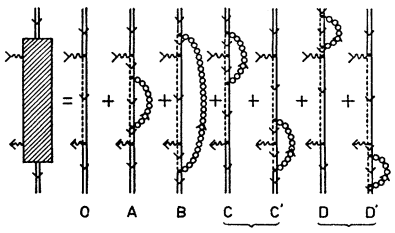

FIG. 4. The general diagram representing the x-ray emission process expressed to first order in the effective interaction between electrons.

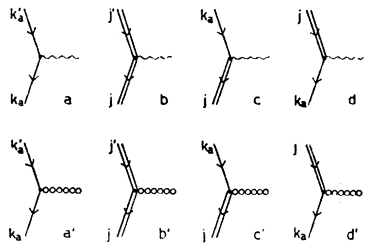

FIG. 5. Basic vertex parts: (a)–(d) vertices for interaction with the radiation field; (a')–(d') vertices of electron-electron interaction.

vertices. In effect, the vertex contributions take either the form $\langle u_j \mid \pm i\mathbf{n}\cdot\nabla \mid u_{j'}\rangle$ for the case where a radiation line (entering or leaving) is connected to the vertex, or the form $\langle u_j \mid \exp(\pm ik_v x) \mid u_{j'}\rangle$ when the vertex contains an interaction line (entering or leaving). Momentum is practically conserved only when both of the states j and j' are conduction states, because, as pointed out in the previous section, one can then replace the OPW functions by plane waves. Then one has

$$\langle u_{\mathbf{k}_a} \mid \mp i\mathbf{n}\cdot\nabla \mid u_{\mathbf{k}_{a'}}\rangle \simeq \pm \mathbf{n}\cdot\mathbf{k}_a \delta_{\mathbf{k}_a,\mathbf{k}_{a'}}, \quad (15a)$$

$$\langle u_{\mathbf{k}_a} \mid \exp\mp i\mathbf{k}_v\cdot\mathbf{x} \mid u_{\mathbf{k}_{a'}}\rangle \simeq \delta_{\mathbf{k}_a \pm \mathbf{k}_v,\mathbf{k}_{a'}}. \quad (15a')$$

In the case where j and j' are both bound states, we write

$$\langle u_j^B \mid \mp i\mathbf{n}\cdot\nabla \mid u_{j'}^B\rangle = 0, \quad (15b)$$

$$\langle u_j^B \mid \exp\mp i\mathbf{k}_v\cdot\mathbf{x}) \mid u_{j'}^B\rangle \equiv g_{jj'}(\pm\mathbf{k}_v). \quad (15b')$$

The zero in Eq. (15b) is a consequence of the selection rules. One can thus immediately discard any diagram containing vertices of that type. In the case where there is one conduction state entering and one core state leaving, we write

$$\langle u_j^B \mid \mp i\mathbf{n}\cdot\nabla \mid u_{\mathbf{k}_a}\rangle \equiv h_{\mathbf{n},j}(\mathbf{k}_a), \quad (15c)$$

$$\langle u_j^B \mid \exp(\mp i\mathbf{k}_v\cdot\mathbf{x}) \mid u_{\mathbf{k}_a}\rangle \equiv f_j(\mathbf{k}_a, \pm\mathbf{k}_v). \quad (15c')$$

If, on the contrary, the core state enters and the conduction state leaves the vertex, one has

$$\langle u_{\mathbf{k}_a} \mid \mp i\mathbf{n}\cdot\nabla \mid u_j^B\rangle \equiv \mp \bar{h}_{\mathbf{n},j}(\mathbf{k}_a), \quad (15d)$$

$$\langle u_{\mathbf{k}_a} \mid \exp(\mp i\mathbf{k}_v\cdot\mathbf{x}) \mid u_j^B\rangle \equiv \bar{f}_j(\mathbf{k}_a, \mp\mathbf{k}_v). \quad (15d')$$

In these expressions, (15a)–(15d'), the states on the left and on the right side of the brackets are represented, respectively, by the lines leaving and entering the vertex, as shown in Fig. 5.

Choosing the Ox_3 axis along the unit vector $\mathbf{n}$ and substituting Eqs. (A1) and (12) into (15b'), (15c), and (15d') one finds

$$g_{ij}(\mathbf{k}) = (2\beta)^6\left[-\frac{6k_ik_j}{(k^2+4\beta^2)^4} + \frac{\delta_{ij}}{(k^2+4\beta^2)^3}\right], \quad (16)$$

$$h_{3i}(\mathbf{k}) = (32/\sqrt{\Omega})(\pi\beta^7)^{1/2}\left[\frac{k_ik_3}{(k^2+\beta^2)^3} - \delta_{i3}H(k)\right], \quad (17)$$

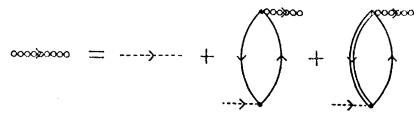

FIG. 6. Integral equation which defines the effective interaction between electrons. The last term is small, and when neglected we regain the effective interaction of the Lindhard approximation (random-phase approximation).

with

$$H(k)=\frac{\alpha^4(2\alpha-\beta Q)}{\beta(\alpha+\beta)^4(k^2+\alpha^2)^2}-\frac{Q(k^2-3\beta^2)}{24(k^2+\beta^2)^3},$$

$$Q=\frac{2[(\alpha+\beta)/2\beta]^4-3[2\alpha/(\alpha+\beta)]^4}{2[(\alpha+\beta)/2\beta]^4-(3\beta/2\alpha)[2\alpha/(\alpha+\beta)]^4},$$

and

$$f_j(\mathbf{k}_a,\mathbf{k}_v)=\bar{u}_j{}^B(\mathbf{k}_a-\mathbf{k}_v)-\sum_i\langle\bar{u}_j{}^B\mid\exp(-i\mathbf{k}_v\cdot\mathbf{x})\mid u_i{}^B\rangle\bar{u}_i{}^B(\mathbf{k}_a). \quad (18)$$

The term $f_j(\mathbf{k}_a,\mathbf{k}_v)$ is particularly cumbersome; however, it is not necessary to express it explicitly. One can show that this function, associated with the mixed vertex c' (or d') of Fig. 5 has an effect which is about 30 times weaker than the Kronecker δ's and $g_{jj'}$ associated with vertex a' and b'. Consequently, we will be able to neglect diagrams containing these mixed vertices. The smallness of $f_j(\mathbf{k}_a,\mathbf{k}_v)$ is due to the orthogonality of the OPW wave functions and the bound states. If $\mathbf{k}_v$ were zero, then Eq. (15c') or (18) would vanish. In fact, the effective potential $V(\mathbf{k}_v,\omega_v)$ is associated with a screening constant $k_{FT}=(4k_0/\pi a_0)^{1/2}=0.78$ a.u. which is considerably smaller than β (and α) as given in Sec. IIIA. To estimate the relative contributions of vertices c' and b' one can expand (15c') and (15b') in powers of k_v/β and $k_a/\beta\simeq k_0/\beta$, where $k_0=0.48$ a.u. is the Fermi wave number.

From Eq. (18), the lowest-order term in $f_j(\mathbf{k}_a,\mathbf{k}_v)$ is

$$f\simeq-5(\pi/\Omega\beta^3)^{1/2}(ik_{vj}/\beta).$$

When summing over states, the $g_{jj'}$ sum is only over the polarizations of the p states while the sum over the k_a in $f_j(k_a,k_v)$ goes over the Fermi sea. An estimate of the relative magnitude after summation is given by

$$\sum_{j'}g_{jj'}\sim1,$$

$$[\sum_{k_a<k_0}f_j(\mathbf{k}_a,\mathbf{k}_v)^2]^{1/2}\sim\{[\Omega/(2\pi)^3]f^2\tfrac{4}{3}\pi k_0{}^3\}^{1/2},$$

but $k_0{}^3=3\pi^2n$, where n is the electron density, and since n is the inverse of the volume v_c of the Wigner-Seitz cell, one has

$$[\sum_{k_a<k_0}f_j(\mathbf{k}_a,\mathbf{k}_v)^2]^{1/2}\sim[(\Omega/2v_c)f^2]^{1/2}\approx0.14k_v/\beta$$

$$\sim0.14k_{FT}/\beta=0.03.$$

An important consequence of smallness of f_j is that the effective potential will almost preserve translation symmetry, i.e.,

$$V(\mathbf{x},\mathbf{x}')\approx V(\mathbf{x}-\mathbf{x}'),$$

and hence possess a Fourier transform of the form

$$V(\mathbf{k},\omega)=v(\mathbf{k})/\epsilon(\mathbf{k},\omega),$$

where $\epsilon(\mathbf{k},\omega)$ is the Lindhard dielectric constant. To see this property more clearly, consider Fig. 6 which represents symbolically the integral equation which defines the effective potential V. The third term contains two mixed vertices. It is therefore weaker than the second term by a factor of about 10^3 and can be neglected. In this case Fig. 6 reduces to the equation defining the effective interaction in the Lindhard approximation. Since the Fourier transform of the effective potential is associated with a single momentum vector, we can attribute this momentum $\mathbf{k}_v$ to the lines of effective interaction (bubble lines).

C. Diagrams Describing Emission

Each of the diagrams of order 0 and 1 on the right of Fig. 4 represents a sum of diagrams described in Fig. 7. In the latter figure we have omitted diagrams containing vertices of type b in accord with rule (iii) of Appendix A and for simplicity we have not drawn the diagrams C' and D' for which the contributions are the same as for the corresponding nonprimed diagrams.

It is useful to estimate the relative magnitudes of the contributions before attempting detailed computations. We will see that among the diagrams of order one, the essential contributions come from A_1, B_1, and C_1. As discussed above, vertices of types c' and d' are small. Of the terms in Fig. 7, only A_1, B_1, C_1, and D_1 have no such vertices; diagrams B_2, C_3, D_3, and D_4 have one d' vertex each; and the other diagrams have two c' and d' vertices each. Thus we expect that only the first term of each series will be significant. To further check this presumption, we should make certain that the contributions from the dominant graphs do not cancel over certain

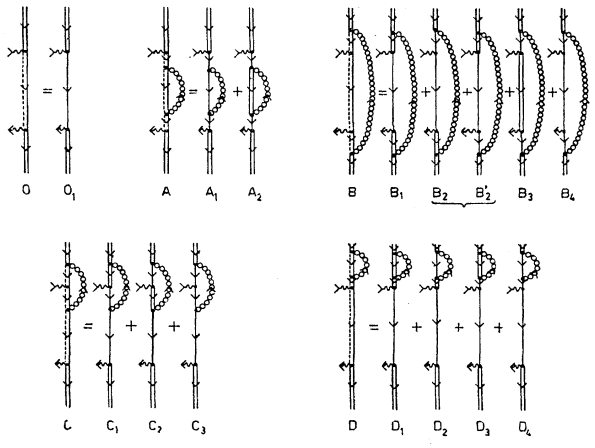

FIG. 7. Nonvanishing contributions to each of the first-order terms in Fig. 4.

regions of the spectrum. In the case of cancellation, the graphs with vertices c' and d' could become important. Indeed, just such a cancellation does occur for the satellite band, as has been remarked previously.[18,19] Notice first of all that the only graphs contributing to the satellite band are diagrams A_1, B_1, B_2, B_4, C_1, and C_3, because these are the only ones giving rise to a final state consisting of a hole in the conduction band plus particle-hole excitations. According to our calculations, the sum of diagrams A_1, B_1, and C_1 turns out to be about 10% of the separate value of any one of these graphs over the satellite band. Thus graphs B_2 and C_3 containing only one vertex d' could be important. However, we can see that these two diagrams are actually down by a factor of 100 and remain negligible. This important factor of 100 arises from the fact that B_1 and C_1 differ respectively from B_2 and C_3 not only by the occurrence of a vertex d', but also by an internal particle line. For the former terms one has a double line (bound state) and has an energy denominator which follows from rule (ii$_b$) of Appendix A of the form $(E_B+\omega_v-E_B)\simeq\omega_v\sim E_F$. The latter terms have this line replaced by a free particle and the corresponding denominator becomes $(E_B+\omega_v-E_k)\simeq E_B$, where ω_v is the frequency transported by the bubble line. The factors E_F and $-E_B$ are in the ratio 1:10. Thus one can neglect B_2 and C_3 in the satellite region, as well as B_4, which contains the two vertices c' and d'. Thus we will be able to neglect all of the diagrams containing vertices c' and d' in the spectral region of interest and it only remains to consider diagrams A_1, B_1, C_1, and D_1 as well as O_1.

Now we must consider the problem of divergences. One can easily see that diagrams D_1 and also D_2 diverge. This results from the second internal line which, according to rule (ii$_b$), gives a contribution $i(E_B-E_B-i\lambda)^{-1}$, which diverges when the adiabatic switching on of the interaction is pushed to the infinite past. This difficulty is a consequence of our approximation method for which the initial state is not an eigenstate of the interacting Hamiltonian. Once the interaction is turned on, the quasilocalized state can decay at any time and the probablility that it survives to the present becomes negligible. However the fact that the soft x-ray spectrum is observed requires that it still exists or at least a memory of it exists at the time of the emission process. In practice, the emission is observed within a brief time interval after the initial state is created. For our purposes, therefore, it is physically more correct to treat the creation of the initial state as occurring at some initial time T and then allowing the state to evolve under the action of electron-electron collisions. Since the interaction effect is strong, it is necessary to go to high order. In the limit as $T\to-\infty$, one finds that, in effect, the energy of the bound state is shifted and the state is given a lifetime. As mentioned in Sec. III A, the shift in E_B only changes the frequency origin and we can assume that the E_B observed in nature is the renormalized value. The state width is found to be small, about 10^{-3} eV. It will be neglected in this article, but we will return to this point in the second article of this series. Therefore for present purposes we can put aside diagrams D_1 and D_2.

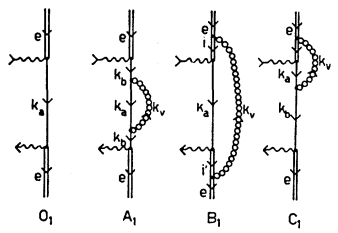

FIG. 8. The important contributions of zero and first order, showing the labeling of lines used in the text.

D. Frequency Integrals

Applying the rules of Appendix A and using the notation shown in Fig. 8, one obtains the following contributions to $F(\omega)$ from graphs O_1, A_1, B_1, and C_1:

$$F_0(\omega)=-(i/2\pi)\int[d\omega'/(\omega'-\omega+i\lambda)]\sum_{\mathbf{k}_a}S_F(\mathbf{k}_a,E_B+\omega')\sum_e|h_{n,e}(\mathbf{k}_a)|^2, \tag{19}$$

$$F_A(\omega)=-[(2\pi)^2\Omega]^{-1}\int[d\omega'/(\omega'-\omega+i\lambda)]\int d\omega_v\sum_{\mathbf{k}_v}\sum_{\mathbf{k}_a,\mathbf{k}_b}V(\mathbf{k}_v,\omega_v)[S_F(\mathbf{k}_b,E_B+\omega')]^2$$
$$\times S_F(\mathbf{k}_a,E_B+\omega'+\omega_v)\delta_{\mathbf{k}_a,\mathbf{k}_b+\mathbf{k}_v}\sum_e|h_{n,e}(\mathbf{k}_b)|^2, \tag{20a}$$

$$F_B(\omega)=-[(2\pi)^2\Omega]^{-1}\int[d\omega'/(\omega'-\omega+i\lambda)]\int d\omega_v\sum_{\mathbf{k}_v}\sum_{\mathbf{k}_a}V(\mathbf{k}_v,\omega_v)[S_B(E_B+\omega_v)]^2S_F(\mathbf{k}_a,E_B+\omega'+\omega_v)$$
$$\times\sum_e|\sum_i h_{n,i}(\mathbf{k}_a)g_{ei}(\mathbf{k}_v)|^2, \tag{20b}$$

$$F_C(\omega)=-[2/(2\pi)^2\Omega]\int[d\omega'/(\omega'-\omega+i\lambda)]\int d\omega_v\sum_{\mathbf{k}_v}\sum_{\mathbf{k}_a,\mathbf{k}_b}V(\mathbf{k}_v,\omega_v)S_B(E_B+\omega_v)S_F(\mathbf{k}_a,E_B+\omega'+\omega_v)S_F(\mathbf{k}_b,E_B+\omega')$$
$$\times\delta_{\mathbf{k}_a,\mathbf{k}_b+\mathbf{k}_v}\sum_{e,i}\bar{g}_{ei}(\mathbf{k}_v)\bar{h}_{n,i}(\mathbf{k}_a)h_{n,e}(\mathbf{k}_b). \tag{20c}$$

Term $F_C(\omega)$ contains an extra factor of 2 to account for the two graphs C_1 and C_1'.

Using the explicit forms given in Eqs. (B2) and (B3) for the particle propagators, and designating by $V_+(\mathbf{k},\omega)$ and $V_-(\mathbf{k},\omega)$ the two parts of $V(\mathbf{k},\omega)$ analytic, respectively, in the upper and lower half of the complex frequency plane, we can carry out the integrations on ω' and ω_v. The $V_\pm(\mathbf{k},\omega)$ have the properties

$$V_+(\mathbf{k},\omega)=V_-(\mathbf{k},-\omega), \tag{21}$$

$$\text{Im } V_+(\mathbf{k},\omega)=0,$$

and

$$\text{Im } V_-(\mathbf{k},\omega)=\text{Im}V(\mathbf{k},\omega), \qquad \text{for } \omega\leq 0, \tag{22a}$$

$$\text{Im } V_+(\mathbf{k},\omega)=\text{Im}V(\mathbf{k},\omega),$$

and

$$\text{Im } V_-(\mathbf{k},\omega)=0, \qquad \text{for } \omega\geq 0. \tag{22b}$$

After integrating, and substituting into Eq. (4) one obtains

$$I_0(\omega)=\tfrac{1}{3}\omega\sum_{\mathbf{k}_a}\eta_{a<}\delta(\omega+E_B-E_a)\sum_e|\,h_{\mathrm{n},e}(\mathbf{k}_a)\,|^2, \tag{23}$$

$$I_A(\omega)=\tfrac{1}{3}\omega(-1/\pi\Omega)\sum_{\mathbf{k}_v}\sum_{\mathbf{k}_a,\mathbf{k}_b}\Big[\eta_{a<}\frac{\partial}{\partial E_b}\Big(\frac{P}{\omega+E_B-E_b}\Big)\text{Im}V_+(\mathbf{k}_v,-\omega-E_B+E_a)$$

$$+\pi\eta_{b<}\frac{\partial\delta(\omega+E_B-E_b)}{\partial E_b}\left[\eta_{a<}\,\text{Re}V_+(\mathbf{k}_v,-\omega-E_B+E_a)-\eta_{a>}\,\text{Re}V_+(\mathbf{k}_v,-\omega-E_B+E_a)\right]\Big]\delta_{\mathbf{k}_a,\mathbf{k}_b+\mathbf{k}_v}\sum_e|\,h_{\mathrm{n},e}(\mathbf{k}_b)\,|^2, \tag{24a}$$

$$I_B(\omega)=\tfrac{1}{3}\omega(-1/\pi\Omega)\sum_{\mathbf{k}_v}\sum_{\mathbf{k}_a}\eta_{a<}\frac{\partial}{\partial E_a}\Big(\frac{P}{\omega+E_B-E_a}\Big)\text{Im}V_+(\mathbf{k}_v,-\omega-E_B+E_a)\sum_e|\sum_i h_{\mathrm{n},i}(\mathbf{k}_a)g_{ei}(\mathbf{k}_v)\,|^2, \tag{24b}$$

$$I_C(\omega)=\tfrac{1}{3}\omega(2/\pi\Omega)\sum_{\mathbf{k}_v}\sum_{\mathbf{k}_a,\mathbf{k}_b}\Big[\eta_{a<}\frac{P}{\omega+E_B-E_a}\frac{P}{\omega+E_B-E_b}\text{Im}V_+(\mathbf{k}_v,-\omega-E_B+E_a)$$

$$-\pi\eta_{a<}\Big(\frac{P}{\omega+E_B-E_b}\Big)\delta(\omega+E_B-E_a)\,\text{Re}V_+(\mathbf{k}_v,0)$$

$$-\frac{\pi\eta_{b<}\delta(\omega+E_B-E_b)}{E_a-E_b}\left[\eta_{a<}\,\text{Re}V_+(\mathbf{k}_v,E_a-E_b)-\eta_{a>}V_-(\mathbf{k}_v,E_a-E_b)\right]\Big]\delta_{\mathbf{k}_a,\mathbf{k}_b+\mathbf{k}_v}\sum_{e,i}\bar{g}_{ei}(\mathbf{k}_v)h_{\mathrm{n},i}(\mathbf{k}_a)h_{\mathrm{n},e}(\mathbf{k}_b). \tag{24c}$$

Some care must be taken in obtaining $I_B(\omega)$ above, and to avoid the appearance of an indeterminate term of the form $[\partial V_+(\mathbf{k},\omega)/\partial\omega]_{\omega=0}$. The derivative is not defined for $\omega=0$ since $\text{Im}V_+(\mathbf{k},\omega)$ increases linearly for $\omega\gtrsim 0$ but vanishes for negative frequencies. In Appendix C, it is shown that the correct prescription is to take this term equal to zero.

However, even with this prescription, term $I_B(\omega)$ remains the most troublesome term of the theory. As we will see, this term diverges logarithmically in the region $|\,E_B\,|<\omega<|\,E_B\,|+E_F$; that is, in the region of the so-called parent band. Thus, with the first-order theory one can only attempt to describe the low-energy features of the spectrum, namely the low-energy tail and the plasmon satellite band. To exhibit this divergence we separate off the factors

$$(1/\Omega)\sum_{\mathbf{k}_a}\eta_{a<}\frac{\partial}{\partial E_a}\Big(\frac{P}{\omega+E_B-E_a}\Big)$$

$$\times\,\text{Im}V_+(\mathbf{k}_v,-\omega-E_B+E_a) \tag{25}$$

(where the principle-value symbol P is actually irrelevant, as shown in Appendix C). When the volume Ω tends to infinity, the sum goes into an integral which can be represented as

$$(1/\Omega)\sum_{\mathbf{k}_a}\eta_{a<}\cdots\xrightarrow[\Omega\to\infty]{}\frac{(2m)^{3/2}}{2(2\pi)^3}$$

$$\times\int d(\text{angles})\int_0^{E_F}dE_a\sqrt{E_a}\cdots.$$

Then Eq. (25) becomes

$$\int_0^{E_F}\frac{dE_a\sqrt{E_a}}{(\omega+E_B-E_a)^2}\,\text{Im}V_+(\mathbf{k}_v,-\omega-E_B+E_a).$$

Using the properties of $\text{Im}V_+(\mathbf{k},\omega)$ around $\omega=0$,

$$\text{Im}V_+(\mathbf{k},\omega)=0, \qquad \text{for } \omega\leq 0$$

$$\text{Im}V_+(\mathbf{k},\omega)\propto\omega, \qquad \text{for } \omega\gtrsim 0$$

then the lower limit of the integral gives contributions

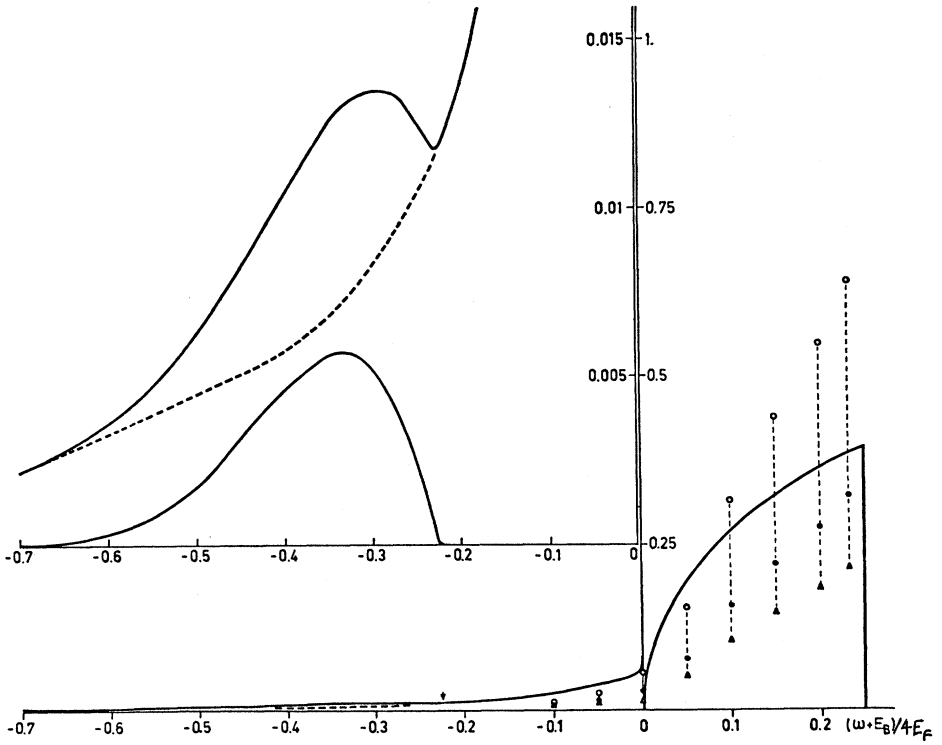

FIG. 9. Calculated results for the soft x-ray emission spectrum of sodium. The main band region of the lower curve is taken from the zero-order (one - electron) theory, while the tailing and satellite band are given to first order in the effective interaction. The curves on the expanded scale to the upper left show the plasmon satellite band by itself and also as added to the low-energy tail. The arrow on the bottom curve marks the high-energy threshold of the satellite. The open circles, black circles, and triangles on the main band curve indicate the position of the observed main band of Crisp (Ref. 13) if the ratio of the intensities of the satellite band and main band is, respectively, 1%, 2%, or 3%. Rooke (Ref. 15) finds a ratio of 2±1%.

of the form

$$\int_{\max(0,\omega+E_B)} \frac{dE_a\sqrt{E_a}}{E_a-(\omega+E_B)}$$

$$=\left[2E_a^{1/2}+(\omega+E_B)^{1/2}\ln\left|\frac{E_a^{1/2}-(\omega+E_B)^{1/2}}{E_a^{1/2}+(\omega+E_B)^{1/2}}\right|\right]_{E_a=\omega+E_B},$$

for $\omega+E_B>0$

$$=\left[2E_a^{1/2}-2(-\omega-E_B)^{1/2}\tan^{-1}\left(\frac{E_a}{-\omega-E_B}\right)^{1/2}\right]_{E_a=0},$$

for $\omega+E_B\leq 0$

which diverges logarithmically for $\omega+E_B>0$. In a subsequent paper[6] we give a more physical explanation of the origin of this divergence and use a renormalized theory to treat the effects of interaction over the whole frequency region. It will also be shown, however, that the conclusions of the first-order theory, in regards to the low-energy portion of the spectrum, retain their validity. Since the first order theory also has the virtue of simplicity, we proceed with the calculation and restrict ourselves to the region $\omega+E_B\leq 0$. The term $I_0(\omega)$ of zero order, will be retained, however, to provide a reference for comparing the intensity of the low-energy features with that of the parent band.

The restriction to $\omega+E_B<0$ simplifies the evaluation of Eqs. (24). Note that the only parts of Eqs. (24) which must be retained are those containing $\mathrm{Im}V_+$. The other terms with $\mathrm{Re}V_\pm$ can be eliminated because they contain the functions $\delta(\omega+E_B-E_a)$ and E_a is always positive. In addition we can ignore the principal-value restrictions P, as well as the index + on $\mathrm{Im}V_+(\mathbf{k},\omega)$ as a consequence of Eqs. (22).

We have been able to carry out analytically all of the integrations over the remaining momentum variables in Eqs. (24) except for the two relating to the arguments of $\mathrm{Im}V_+$. These last two integrals were performed numerically with the aid of the IBM 7094 computer of the University of Maryland. The results are given in Fig. 9. To the left of the vertical axis there is the curve $I_A(\omega)+I_B(\omega)+I_C(\omega)$. This curve could not be given to the right of the axis, i.e., in the region where $I_0(\omega)\neq 0$, as a consequence of the divergence in $I_B(\omega)$.

IV. SUMMARY AND DISCUSSION

The results shown in Fig. 9 can be compared with the experimental spectra indicated in Fig. 2. The experimental plasmon emission satellite of sodium has not yet appeared in the literature, but Rooke[15] claims its form is similar to the satellite shown for aluminium, and its maximum intensity as a percentage of the intensity at the corresponding place in the parent band is 2±1%. The plotted points appearing in Fig. 9 have been put in as a measure of this relative intensity. The points reproduce the Crisp and Williams spectrum for the parent band drawn to three scales such that the plasmon band is 1, 2, or 3% of the parent band. It is seen that our results indicate a staellite band of about 1.5%. However, this conclusion must be qualified by the fact

TABLE I. Contributions to the soft x-ray emission intensity $I/m\omega$ from the important graphs of the first-order theory.

$w=(\omega+E_B)/4E_F$	Tailing A_1	B_1	C_1	Total	Satellite A_1	B_1	C_1	Total	Total
−0.70	0.3206	0.8184	−0.9176	0.2214	0	0	0	0	0.2214
−0.65	0.4492	1.0755	−1.2484	0.2762	0.0378	0.0726	−0.1036	0.0069	0.2831
−0.60	0.5792	1.3190	−1.5633	0.3349	0.1934	0.3411	−0.5032	0.0312	0.3661
−0.55	0.7004	1.5390	−1.8433	0.3961	0.6217	0.9942	−1.5324	0.0835	0.4795
−0.50	0.7885	1.7109	−2.0440	0.4555	1.8040	2.5420	−4.1686	0.1774	0.6329
−0.45	0.7956	1.7921	−2.0835	0.5042	6.0141	7.0609	−12.7516	0.3233	0.8276
−0.40	0.8380	1.9497	−2.2120	0.5756	8.7247	9.6414	−17.9032	0.4630	1.0387
−0.35	0.9359	2.2081	−2.4625	0.6815	10.3722	10.9522	−20.7580	0.5664	1.2479
−0.30	1.0748	2.5560	−2.8023	0.8286	10.7306	10.9053	−21.1079	0.5279	1.3565
−0.25	1.2657	3.0191	−3.2470	1.0377	8.3643	8.3196	−16.4490	0.2349	1.2727
−0.20	1.5294	3.6293	−3.8145	1.3442	0	0	0	0	1.3442
−0.15	1.9170	4.4579	−4.5533	1.8216					
−0.10	2.5842	5.7006	−5.6164	2.6685					
−0.075	3.1687	6.6153	−6.3785	3.4055					
−0.05	3.3952	7.9065	−7.4399	3.8619	the satellite vanishes for				See total
−0.04	3.4871	8.6534	−7.9562	4.1845	$w<-z_c(1+z_c)=-0.6954$				tailing
−0.0256	3.6511	10.0094	−9.0282	4.6323	$w>\frac{1}{4}-(\hbar\omega_p/4E_F)=-0.2198$ [a]				
−0.0144	3.7909	11.5808	−10.2723	5.0995					
−0.0064	3.9721	13.3849	−11.7080	5.6492					
−0.0016	4.0442	15.4426	−13.1921	6.2947					
0	4.6311	17.3720	−13.5844	8.4188					

w	Main BD. (0 order)
0	0
0.0016	3.594
0.0064	7.170
0.0144	10.710
0.0256	14.198
0.0400	17.617
0.0900	25.755
0.1225	29.553
0.1600	33.138
0.2025	36.492
0.2500	39.601
>0.25	0

[a] See Ref. 12.

that the parent band in Fig. 9 is the zero-order result, since the first-order theory, used for the satellite band, could not be extended into this region. The plasmon-band threshold is shifted down in energy by the expected $\hbar\omega_p$ from the high-energy edge of the parent band. This energy is the minimum which must be left behind in the metal in order to set up the plasmon excitation. The shape of the satellite is broader and its peak is shifted to lower relative energy than that of the parent band. These changes are primarily due to the wave-number dependence (dispersion) of the plasmon frequency, and a cancellation between terms of the perturbation theory, as discussed below. Hedin[20] has recently suggested that the satellite has additional structure introduced by a mode which he calls the plasmaron. The first-order theory does not contain this effect, but there is some evidence for it from the renormalized theory.[6]

The order of magnitude of the tailing and its slope can be compared with that of the main band and the plasmon satellite. The tailing comes from the continuum of one-electron excitations which can be set up in the metal. In the region of the plasmon satellite, the theoretical tailing intensity is of the same order of magnitude as that of the satellite. It would be of interest to make a detailed comparison of these features with the experimental curves, but it will first be necessary to obtain more reliable data from which one can separate off extraneous background intensity.

In determining these spectra it has been found that there is a strong cancellation among the contributions to the first-order theory. As shown in Table I, the cancellation is strongest for the plasmon satellite band in which case it reduces the maximum intensity by a factor of about 20. Term A_1 of Figs. 7 or 8 accounts for the interaction between electrons in the conduction band. As such, this process can be associated with Landsberg's[7] treatment, discussed in the Introduction. The present treatment is more general in that Landsberg used a static screened potential which does not allow for plasmon production. Term B_1 of Figs. 7 or 8 describes the excitation of a conduction band electron by the hole in the core state. The hole acts as a positively charged impurity in the metal which can excite conduction band electrons virtually. When the x ray is subsequently emitted, it has a lowered energy since some energy is left behind to make the virtual excitations real. This process is not unrelated to that considered by Pirenne and Longe[8] in a static approximation. In their treatment the virtual excitation is interpreted as a component of a conduction electron wave function which is modified

prior to the x-ray emission by the presence of the core-state hole. The symmetry of the graphs A_1 and B_1 about their intermediate state [the final state in the sense of Eq. (2)] shows that these terms are positive definite. The terms C_1 and C_1', however, do not have this symmetry. They are interference terms made up of a cross product between a matrix element for core excitation of the conduction band and one for interaction between conduction electrons. These terms are strongly negative and are very important for reducing the plasmon satellite intensity to the correct order of magnitude. Ferrell[17] showed that cancellation causes the satellite spectrum to behave like $E^{3/2}$ measured down from its high-energy edge. This behavior though analytically correct, may be difficult to observe, since our numerical results show a faster rise even quite close to the edge. The cancellation is not so complete for the spectrum of the tailing, but Table I shows that the interference term is nevertheless of major importance. It seems to have been overlooked in previous treatments of the emission process.

The major shortcoming of the present theory is that it cannot be extended into the region of the parent band. It was shown in Sec. III D that term B_1 diverges logarithmically over the whole parent band, and it can also be shown that terms C_1 diverge at the high-energy edge. In addition, even if these terms were finite, the low-energy threshold of the zero-order term would lead to a discontinuity of slope in the combined zero- and first-order theory. The discontinuity is probably not physical, and appears due to the limitations of perturbation theory for treating phenomena near thresholds. Higher-order terms can be expected to diverge at this point. Consequently, the calculated tailing spectrum may not be reliable close to the edge and probably increases more rapidly than the actual spectrum.

These difficulties can be removed by going to a renormalized theory in which the basic electron states and the core hole are replaced by quasiparticles which are always considered along with their clouds of interacting particles. Some effects of this kind have been considered by Hedin[20] and others and will be described more fully in a subsequent article.[6] It will be seen that the renormalization introduces additional structure into the spectrum. However, several basic features of the result are already apparent in first order. These include the imprtance of the interference between terms due to core excitation and conduction-band interaction, the relative order of magnitude of the tailing of the spectrum and the plasmon satellite band, and the structure of the satellite band in comparison with the parent band from which it originated.

ACKNOWLEDGMENTS

We would like to thank all the people with whom we had interesting and useful conversations, especially R. A. Ferrell, J. Friedel, J. Pirenne, F. Brouers, S. M. Bose, and G. A. Rooke. Computer time for this project was supported in part by the National Aeronautics and Space Administration under Grant No. NsG 398 to the Computer Science Center of the University of Maryland, and by the Computer Science Center of the University of Liège. P.L. would also like to thank the Fulbright Foundation and the Institut Inter-universitaire des Sciences Nucléaires of Belgium for several travel grants and the University of Maryland for support and hospitality.

APPENDIX A: $\mathbf{u}_i(\mathbf{x})$ FOR SODIUM

Using units of inverse Bohr radii (i.e., a.u.), Slater's rules[23] provide shielding constants of the form $(Z-s)/n^*$. Here $Z=11$. For a $1s$ state, $n^*=1$ and $s=0.30$, which provides a shileding constant $\alpha=10.7$. For the states $2s$ and $2p$, one has $n^*=2$ and $s=0.85\times2+0.35\times7=4.15$, which gives a screening constant $\beta=3.425$. The corresponding core wave functions then become, after orthornormalization,

$$u_{1s}{}^B(\mathbf{x})=(\alpha^3/\pi)^{1/2}[e^{-\alpha r}], \tag{A1a}$$

$$u_{2s}{}^B(\mathbf{x})=\frac{(\alpha+\beta)^4}{(4\pi D)^{1/2}}[re^{-\beta r}]-\frac{3(2\alpha)^3}{(4\pi D)^{1/2}}[e^{-\alpha r}], \tag{A1b}$$

with

$$D=3(\alpha+\beta)^8/(4\beta^5)-18(2\alpha)^3;$$

and

$$u_{2p,i}{}^B(\mathbf{x})=(\beta^5/\pi)^{1/2}(x_i/r)[re^{-\beta r}], \tag{A1c}$$

with

$$r=(x_1{}^2+x_2{}^2+x_3{}^2)^{1/2}.$$

The Fourier transforms of Eqs. (A1) become

$$u_{1s}{}^B(\mathbf{k})=\frac{8\pi}{\sqrt{\Omega}}\left[\left(\frac{\alpha^3}{\pi}\right)^{1/2}\frac{\alpha}{(k^2+\alpha^2)^2}\right], \tag{A2a}$$

$$u_{2s}{}^B(\mathbf{k})=\frac{8\pi}{\sqrt{\Omega}}\left[\frac{(\alpha+\beta)^4}{(4\pi D)^{1/2}}\frac{(-k^2+3\beta^2)}{(k^2+\beta^2)^3}-\frac{3(2\alpha)^3}{(4\pi D)^{1/2}}\frac{\alpha}{(k^2+\alpha^2)^2}\right], \tag{A2b}$$

$$u_{2p,i}{}^B(\mathbf{k})=\frac{8\pi}{\sqrt{\Omega}}\left[\left(\frac{\beta^5}{\pi}\right)^{1/2}\frac{(-4i\beta k_i)}{(k^2+\beta^2)^3}\right]. \tag{A2c}$$

The conduction wave functions are obtained by substitution of Eqs. (A1) and (A2) into (12) and (13). In the neighborhood of the origin, Eq. (13) takes the form

$$u_{\mathbf{k}}(\mathbf{x})=(\sqrt{\Omega})^{-1}\left[e^{i\mathbf{k}\cdot\mathbf{x}}-\frac{(2\alpha)^4}{2(k^2+\alpha^2)^2}e^{-\alpha r}+\frac{2}{D}\left(\frac{(\alpha+\beta)^4(k^2-3\beta^2)}{(k^2+\beta^2)^3}+\frac{3(2\alpha)^4}{2(k^2+\alpha^2)^2}\right)\times[(\alpha+\beta)^4re^{-\beta r}-3(2\alpha)^3e^{-\alpha r}]-\frac{32i\beta^6}{(k^2+\beta^2)^3}(\mathbf{k}\cdot\mathbf{x})e^{-\beta r}\right]. \tag{A3}$$

APPENDIX B: DIAGRAMMATIC RULES FOR F(ω)

1. Rules for External Lines

(i_a) The two double lines are associated with the same state index j as well as the same energy E_B. The two wavy (radiation) lines are associated with the same frequency ω'.

(i_b) The combined contribution from all of these lines to each graph is a factor

$$-(i/2\pi)(\omega'-\omega+i\lambda)^{-1}. \tag{B1}$$

2. Rules for Internal Lines

(ii_a) The internal particle lines are each associated with either a distinct discrete state index for each double line, or with a momentum, for a single directed line. Similarly, the interaction lines (lines of bubbles) are assigned a momentum and a direction. Each internal line is associated with an energy (or frequency with $\hbar=1$) in such a way as to conserve the energy entering and leaving each vertex.

(ii_b) The internal lines contribute the following factors

For a single line with indices ($\mathbf{k}_a, \omega$) (i.e., with momentum $\mathbf{k}_a$ and energy ω), a factor

$$S_F(\mathbf{k}_a, \omega)=\frac{i\eta_{a>}}{\omega-E_a+i\lambda}+\frac{i\eta_{a<}}{\omega-E_a-i\lambda}; \tag{B2}$$

for a double line with indices (j, ω), a factor

$$S_B(\omega)=i/(\omega-E_B-i\lambda); \tag{B3}$$

for an interaction line with indices ($\mathbf{k}_v, \omega$), a factor

$$(2\pi i\Omega)^{-1}V(\mathbf{k}_v, \omega), \tag{B4}$$

where Ω is the volume of the system. The single-particle energies for the conduction band are taken as $E_a=\mathbf{k}_a^2/(2m)$, and λ is a positive infinitesimal. The η's are the step functions

$$\begin{aligned}\eta_{a>}&=0, \quad \text{for } E_a\leq E_F\\ &=1, \quad \text{for } E_a>E_F,\end{aligned} \tag{B5}$$

and

$$\eta_{a<}=1-\eta_{a>}.$$

3. Rules for Vertices

(iii_a) For a vertex which terminates an interaction line with indices ($\mathbf{k}_v, \omega$) there is a factor

$$\langle l \mid \exp(\pm i\mathbf{k}_v\cdot\mathbf{x}) \mid m\rangle, \tag{B6}$$

where the incoming state is $\mid m\rangle$ and the outgoing state $\mid l\rangle$. The incoming and outgoing states can be either a conduction-band state so that $\mid m\rangle=\mid k_m\rangle$, where $\mid k_m\rangle$ is given by Eq. (A3) of the text, or a localized state $\mid m\rangle=\mid B_m\rangle$, where for sodium $\mid B_m\rangle$ is the $u_{2p,m}{}^B(\mathbf{x})$ of Eq. (A1c). The sign of the exponent in Eq. (B6) is chosen in accord with the direction assignment of rule (ii_a) so that the positive sign is for $\mathbf{k}_v$ directed into the vertex.

(iii_b) For a vertex of interaction with the radiation field, where the incoming particle state is $\mid m\rangle$ and the outgoing state is $\mid l\rangle$, there is a factor

$$\langle l \mid \pm\mathbf{n}\cdot\mathbf{p} \mid m\rangle, \tag{B7}$$

where $\mathbf{p}$ is the momentum operator $\hbar\nabla/i$ and $\mathbf{n}$ is the unit polarization vector of the electromagnetic field. The sign of Eq. (B7) is chosen positive if the radiation is emitted and negative for absorption.

4. Rules for Sums Over States

(iv_a) Integrate all frequencies except ω over the domain $(-\infty, \infty)$.

(iv_b) Sum over all discrete indices of the bound states and sum over all momenta of the conduction states and interactions. The latter sums can be changed to integrals in the usual way with

$$\sum_{k_a}\rightarrow(\Omega/8\pi^3)\int d^3k_a.$$

APPENDIX C: DESCRIPTION FOR FREQUENCY INTEGRAL OF $I_B(\omega)$

After integrating on ω' in $F_B(\omega)$ as given by Eq. (20b), the next step is to carry out the integral on ω_v and extract the real part in accord with Eq. (3). The frequency integral then takes the form

$$\begin{aligned}&\mathrm{Re}(-2\pi i)\int d\omega_v\eta_{a<}V(\mathbf{k}_v, \omega_v)[S_B(E_B+\omega_v)]^2\\ &\qquad\times S(\mathbf{k}_a, E_B+\omega+\omega_v)\\ &=\lim_{\epsilon\rightarrow 0}(2\pi)^2\eta_{a<}\,\mathrm{Im}\frac{\partial}{\partial\epsilon}\frac{V_+(\mathbf{k}_v, \epsilon)-V_+(\mathbf{k}_v, -\omega-E_B+E_a)}{\omega+E_B-E_a+\epsilon-i\lambda}\\ &=\lim_{\epsilon\rightarrow 0}(2\pi)^2\eta_{a<}\frac{\partial}{\partial\epsilon}P\\ &\qquad\times\frac{\mathrm{Im}V_+(\mathbf{k}_v, \epsilon)-\mathrm{Im}V_+(\mathbf{k}_v, -\omega-E_B+E_a)}{\omega+E_B-E_a+\epsilon},\end{aligned} \tag{C1}$$

where ϵ is a real parameter. The passage to the limit

appears to give an indeterminant for form since

$$\partial \operatorname{Im} V_+(\mathbf{k}_v, \epsilon)/\partial\epsilon$$

is not defined at $\epsilon=0$. However, we will show that this derivative can be taken to have zero value at this point. Going back to the definition of V, as shown in Fig. 6, we can write

$$V(\mathbf{k}_v, \omega) = v(\mathbf{k}_v) \sum_{n=0}^{\infty} [-B(\mathbf{k}_v, \omega) v(\mathbf{k}_v)]^n, \quad \text{(C2)}$$

where, in the Lindhard approximation, $B(\mathbf{k}_v, \omega)$ represents a simple bubble with two vertices and is given by

$$B(\mathbf{k}_v, \omega) = (2/\Omega) \sum_{\mathbf{k}_b, \mathbf{k}_c} \delta_{\mathbf{k}_b, \mathbf{k}_c + \mathbf{k}_v} \times \left(\frac{\eta_{b<}\eta_{c>}}{\omega - E_b + E_c - i\lambda} - \frac{\eta_{b>}\eta_{c<}}{\omega - E_b + E_c + i\lambda} \right). \quad \text{(C3)}$$

The function $B(\mathbf{k}_v, \omega)$ has analytic properties which are similar to those of $V(\mathbf{k}_v, \omega)$ including those of Eqs. (21) and (22), and has an angular point at $\omega=0$. Substituting $B(\mathbf{k}_v, \omega)$ for $V(\mathbf{k}_v, \omega)$ in Eq. (B1), i.e., using the first-order term of Eq. (C2) for V, enables us to perform the ω_v integral explicitly, with the result

$$\operatorname{Re}(-4\pi/\Omega)[v(\mathbf{k}_v)]^2 \sum_{\mathbf{k}_b, \mathbf{k}_c} \delta_{\mathbf{k}_b, \mathbf{k}_c + \mathbf{k}_v} \int \frac{d\omega' \eta_{a<}}{(\omega_v - i\lambda)^2 (\omega_v + \omega + E_B - E_a - i\lambda)} \left(\frac{\eta_{b<}\eta_{c>}}{\omega_v - E_b + E_c - i\lambda} - \frac{\eta_{b>}\eta_{c<}}{\omega_v - E_b + E_c + i\lambda} \right)$$

$$= (8\pi^2/\Omega)[v(\mathbf{k}_v)]^2 \sum_{\mathbf{k}_b, \mathbf{k}_c} \delta_{\mathbf{k}_b, \mathbf{k}_c + \mathbf{k}_v} \operatorname{Im} \frac{\eta_{a<}\eta_{b>}\eta_{c<}}{(E_b - E_c - i\lambda)^2 (\omega + E_B - E_a + E_b - E_c - i\lambda)}. \quad \text{(C4)}$$

The η functions show that always $E_b \neq E_c$, and one can set $\lambda \to 0$ in the factor $(E_b - E_c - i\lambda)^{-2}$. It is precisely the redundant λ which causes the difficulty in Eq. (C1). Using Eq. (C3), one can rewrite the result in Eq. (C4) as

$$(2\pi)^2 \eta_{a<} \operatorname{Im}[-v(\mathbf{k}_v) B(\mathbf{k}_v, -\omega - E_B + E_a) v(\mathbf{k}_v)]/(\omega + E_B - E_a)^2.$$

In second and successive orders, we can also carry out the integration in terms of the $B(\mathbf{k}_v, \omega)$'s. Comparison with Eq. (C1) shows that we get the same result if we simply set the term $\operatorname{Im} V_+(\mathbf{k}_v, \epsilon) = 0$. Equivalently, we can replace Eq. (C1) by

$$(2\pi)^2 \eta_{a<} \operatorname{Im} V_+(\mathbf{k}_v, -\omega - E_B + E_a) \frac{\partial}{\partial E_a} \frac{P}{\omega + E_B - E_a}.$$